Remote Sensing of Spacecraft Potential at Geosynchronous Orbit using Secondary and Photo Electrons

Miles T. Bengtson * and Hanspeter Schaub†
University of Colorado, Boulder, CO, 80309

Various methods have been proposed for remotely sensing the surface potential of a space object. One such method involves measuring the energy distribution of secondary or photo-electrons emitted from the target and captured by a co-orbiting craft. Assuming the servicing craft can actively control its potential to be at a large positive value relative to the target, the low energy electrons emitted by the target are accelerated toward the servicing craft and arrive with an energy equal to the potential difference between the two craft plus the initial energy of the electrons. The servicing craft measures the electron energy spectrum and, knowing its own potential, then infers the potential of the target. This paper presents experimental results to quantify the energy distribution as a function of angle and total number of secondary electrons emitted from various materials when bombarded by energetic electrons under conditions representative of Geosynchronous Earth Orbit. A similar experiment is conducted to measure the photoelectron population when various materials are exposed to a solar simulator light. The results of this work are important for understanding the physics of remote potential sensing using particles and further developing the technology for application to on-orbit missions.

I. Introduction

The ability to remotely sense the potential on a spacecraft surface is an enabling technology for a range of applications including orbital servicing and docking, close proximity flying, as well as electrostatic (Coulomb) actuation. Though spacecraft charging has been studied for decades, limited work has been done on how to sense and monitor the charge on a spacecraft. This paper presents experimental progress on one such technique in which a co-orbiting satellite measures the energies of electrons which are emitted from a target object to determine the target's surface potential.

Spacecraft charging has historically been viewed as a hazard to be mitigated. In geosynchronous Earth orbit (GEO) satellites can charge to kilovolt levels, and electrostatic discharge is thought to be a common cause of satellite anomalies [1, 2]. Therefore, it would be advantageous to conduct on-orbit investigations of spacecraft under natural and forced charging to better understand how charging affects satellite operations and longevity. Several studies show that astronauts or other objects operating in the wake of the International Space Station could charge to dangerously high potentials [3, 4]. Many future space missions propose complex rendezvous, servicing, assembly, and other proximity operations between multiple craft (e.g. [5–7]). Interactions between satellites charged to different levels could result in hazardous discharges. Therefore, the ability to touchlessly measure the potential on an object would be extremely beneficial for ensuring the safety and robustness of future space operations.

Numerous space missions have recently been proposed which seek to leverage electrostatic forces and torques between multiple charged spacecraft, rather than mitigating the charging. The Electrostatic Tractor or ET is an elegant concept for tugging space debris in GEO using Coulomb forces which has significantly less risk than alternatives that require physical contact [8]. Reference [9] investigates how a charged tractor satellite can be used to arrest the rotation of large debris from a safe distance. Other concepts propose using Coulomb forces to maintain relative positioning in multiple-craft formations [10]. For these and other missions scenarios involving proximity operations between charged objects, it is critical to be able to measure the potential on an object from a distance.

Ferguson [11] was the first to propose the concept of remote potential sensing from either the ground or a co-orbiting satellite. Most of the methods under investigation involve measuring the x-rays or particles emitted from the target surface, which allows the surface potential to be inferred. The Autonomous Vehicle Systems (AVS) Laboratory at the University of Colorado is investigating two different methods for measuring the potential of a surface in space from a satellite orbiting near the target object. Both methods involve firing an electron beam at the target object. When the energetic electrons impact the surface, they produce bremmstrahlung x-rays and secondary electrons. The wavelength

*Graduate Research Assistant, Aerospace Engineering Sciences Department, 431 UCB, AIAA Member
†Professor, Aerospace Engineering Sciences Department, 431 UCB, AIAA Associate Fellow

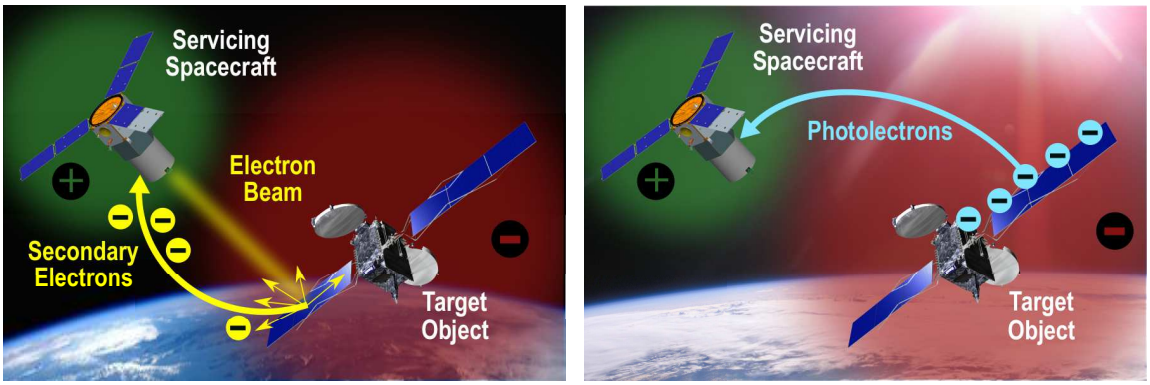

(a) Forced charging scenario in which an electron beam transfers charge and generates secondaries which are used for sensing.

(b) Natural charging scenario in which photoelectrons are used for sensing.

Fig. 1 Concept of operations in which a servicing craft touchlessly measures the potential of a target using either secondary or photo electrons.

of the bremmstrahlung x-rays is proportional to the landing energy of the electrons. Therefore, if the initial energy of the electron beam is known, the x-rays can be used to determine the landing energy, and the potential of the target craft can be inferred. Reference [12] discusses the bremmstrahlung method in full detail.

The current research builds on previous work which investigates the prospects and challenges of using secondary electrons to measure the potential of a surface [13]. Energetic electrons which impinge upon a surface generate secondary electrons which have very low energy (a few eV). Similarly, sunlight acting on a surface will liberate low energy photoelectrons (also at a few eV). If the servicing satellite is charged positive relative to the surface being measured, the electrons are accelerated toward the servicing craft and arrive with an energy equal to the potential difference between the two craft. Therefore, if the servicing satellite measures its own potential relative to the plasma, a process which is well established (e.g. [14]), the potential of the target object can be inferred. A mission concept is presented in Figure 1. A servicing craft approaches a target object which has an unknown potential. Depending on the situation, the servicing craft either directs an electron beam at the target or positions itself in view of the sunlit surfaces. The servicing craft changes its potential (via electron emission) to be large positive. Secondary or photoelectrons generated on the target object are accelerated toward the servicing craft and measured with an electron energy analyzer. The potential of the target object is then inferred. Note the electron beam will change the charge state of the target, so this technique is only applicable to forced charging scenarios in which an electron beam is already being used to transfer charge. Observing photoelectrons will not change the charge state of the object, so it is relevant for passive sensing applications. It should be noted that although the touchless sensing concept is novel, the hardware required for an on-orbit mission has extensive flight heritage.

References [15–17] present how electron energy data from Lunar Prospector is used to remotely determine the potential and electric fields on the surface of the Moon. These results demonstrate that the technique is feasible; however, this work differs in that the separation between target and servicing spacecraft is much larger. Such distances are possible in this case because the Moon is large, so the electron population is easily measurable. Reference [13] shows that the technique can be applied between two spacecraft in geosynchronous orbit over distances of tens of meters.

This work presents experimental results of secondary and photo electron emission from a flat surface held at a fixed potential. Various materials are considered, including aluminum, copper, titanium, aluminized polyimide, and indium tin oxide. Additionally, angular-resolved measurements are presented to illustrate the relative geometries for which the technique is feasible. The paper is organized as follows. Section II summarizes the the questions which motivated the experimental campaign. Section III details the experiment setup and equipment. Results are presented and discussed in Section IV.

II. Experiment Motivation

The touchless potential sensing concept is complicated by several factors. First, secondary and photo electrons are emitted from a surface with a distribution of energies. For secondaries, the peak in the distribution occurs at an energy equal to one third of the work function [18]. For photoemission, the electrons have an energy equal to the energy of the photon minus the work function of the surface. Electrons which leave the surface with approximately 0 eV arrive at the sensing craft with an energy exactly equal to the potential difference between the two craft. However, the initial electron energy distribution will have an effect of widening and shifting the measured peak slightly higher than the nominal potential difference between the two craft. This effect will be minimized as the potential difference between the target and servicing craft becomes large.

Furthermore, the presence of oxide layers, contaminants, and variations in surface roughness can effect the emission characteristics of a surface. Whereas many studies consider materials that are high grade and rigorously cleaned, the characteristics of technical materials, or materials from which spacecraft are actually built, can vary significantly from the "nominal" material properties due to these effects [19]. The purpose of this study is not to measure precisely the properties of the materials under consideration, but rather to investigate whether secondary and photo electrons can be used to touchlessly measure the potential of a spacecraft surface.

Finally, the shapes and relative geometries of the target object and sensing craft play a large role in the feasibility of remote potential sensing. Secondary electrons are emitted from a surface with a cosine angular distribution [20]. For scenarios in which the potential difference between the two craft is on the same order as the initial energy of the electrons (for example, volts or tens of volts), the initial angular distribution of the secondaries has an effect on the number of particles which are measured at the sensing craft [13]. If the potential difference is significantly larger (100s of volts or kilovolts), the electron motion is determined by the electric field, which is in turn strongly dependent on the shape of the target and sensing craft.

In light of these considerations, four primary questions were defined to be answered by the experiments:

1) Can an electron beam generate a sufficient number of secondary electrons for touchless measurement of surface potential?
2) Can solar light generate enough photoelectrons for touchless measurement of surface potential?
3) How do material properties affect the ability to touchlessly measure surface potential? Specific properties to be considered include the presence and characteristics of oxide layers, the presence of surface contaminants, and electron yields.
4) For what relative geometries between the target and the sensor is touchless measurement of potential possible?

III. Experiment Setup

The experimental campaign was carried out in two separate facilities and over two separate times due to equipment availability and scheduling constraints. The first experiment was conducted from June-August 2018 in the Minion vacuum chamber in the Spacecraft Charging and Instrument Calibration Laboratory (SCICL) at the Air Force Research Laboratory, Kirtland Air Force Base, New Mexico. The primary focus of this experiment was to determine over what angles relative to the surface normal the electrons could be measured. A copper plate was used as a target, and the electron energy analyzer was mounted on a rotating arm controlled by a stepper motor that swept from the surface normal to 90° from normal. The copper target was biased to various negative potentials.

The second experiment was conducted from September-November 2018 in the Electrostatic Charging Laboratory for Interactions between Plasma and Spacecraft (ECLIPS) chamber in the AVS Laboratory at the University of Colorado Boulder. This experiment focused on how materials with different emission characteristics affect the touchless sensing process. A vacuum ultraviolet (VUV) lamp was used to investigate the feasibility of sensing with photoelectrons, in place of secondaries produced by an electron beam. Several common spacecraft materials were used, including 110 copper, 6061 aluminum, titanium, aluminized polyimide, and indium tin oxide (ITO) coated glass. The titanium was cleaned with dish soap and water to remove grease. The copper was cleaned with vinegar to remove oxidized oils on the surface. The copper, aluminum, and titanium were additionally cleaned with isopropyl alcohol prior to being placed in vacuum. The aluminized polyimide sample consisted of a 0.3 mil thick sheet of Kapton film coated with a 100 nm thick layer of aluminum. The sample was secured to an aluminum backing plate with polyimide tape for mounting in the experiment fixture. The ITO sample consisted of a 150-300 Å thick layer of ITO deposited on a glass slide, which was also affixed to an aluminum backing plate with polyimide tape for mounting.

Table 1 gives details about the specific equipment used in each experiment. The chambers used in each part of the experiment are identical in size and shape. The vacuum ultraviolet (VUV) source emits primarily between 160 and

Table 1 Equipment and specifications for both experimental campaigns.

Item	SCICL	ECLIPS
Electron Gun	Kimball Physics EFG-7	Kimball Physics EMG-4212C
Instrument Power Supply	Textronix PWS4602	Keithley 2231A-30-3
Plate Bias Power Supply	Keithley 6517B	Keithley 2231A-30-3
Current Meter	Keithley 6430	Keithley 2401 SourceMeter
Typical Vacuum Pressure	10^{-6} torr	10^{-6} torr
Ultraviolet Light	-	Hamamatsu L10706

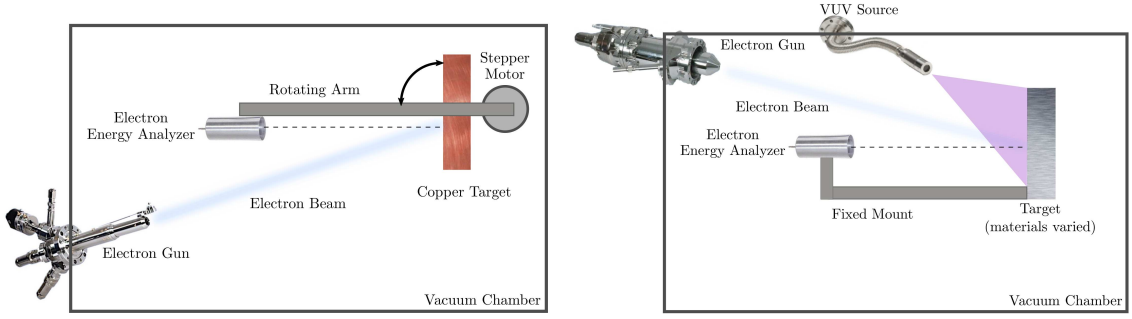

(a) Experiment setup in Minion at AFRL. **(b) Experiment setup in ECLIPS in the AVS Laboratory.**

Fig. 2 Schematics of both parts of the experimental campaign. The experiment conducted at AFRL included rotational motion of the electron energy analyzer. The experiment conducted in the AVS Laboratory was static, though an ultraviolet source was included and various materials were considered.

170 nm. Figure 2 shows schematics of the components in each experiment. Figure 3 provides pictures of each setup in the vacuum chambers. The EMG-4212C electron gun was operated to emit electrons at an energy of 1.5 keV and an emission current of approximately 40 μA. The EFG-7 electron gun was operated at an energy of 300 eV with an emission current of 10 μA.

A custom Gridded Faraday Cup (GFC) was used for each experiment. The first grid was biased to -10 V to exclude electrons from any sources other than the plate (for example, secondary electrons from other surfaces in the chamber). The second grid was swept from 0 V to negative tens of volts to determine the electron energy distributions. Identical copper grids with a mesh size of 70 were used in the GFC for each experiment.

IV. Experiment Results and Discussion

A. Material Considerations

Experimental results for copper, aluminum, titanium, aluminized Kapton, and ITO, under illumination from the electron gun and VUV source, are shown in Figures 4 through 13. In each case, the target plate was biased to either -15 V or -20 V. Ideally, all of the generated electrons have energies of the potential applied to the plate plus some small initial energy. Therefore, by sweeping through voltages on the energy analyzer discriminator grid, a step decrease in detector current is expected when the grid voltage is equal to the plate voltage. Much of the data was noisy, so the following smooth step-function model was fit to each of the datasets:

$$I = a - b\tanh(cV + d), \tag{1}$$

where I is the current, V is the discriminator grid voltage, and a, b, c, and d are fitting constants. The constants were determined using the `nlinfit` function in Matlab. Taking the negative derivative of the I-V curve gives the energy

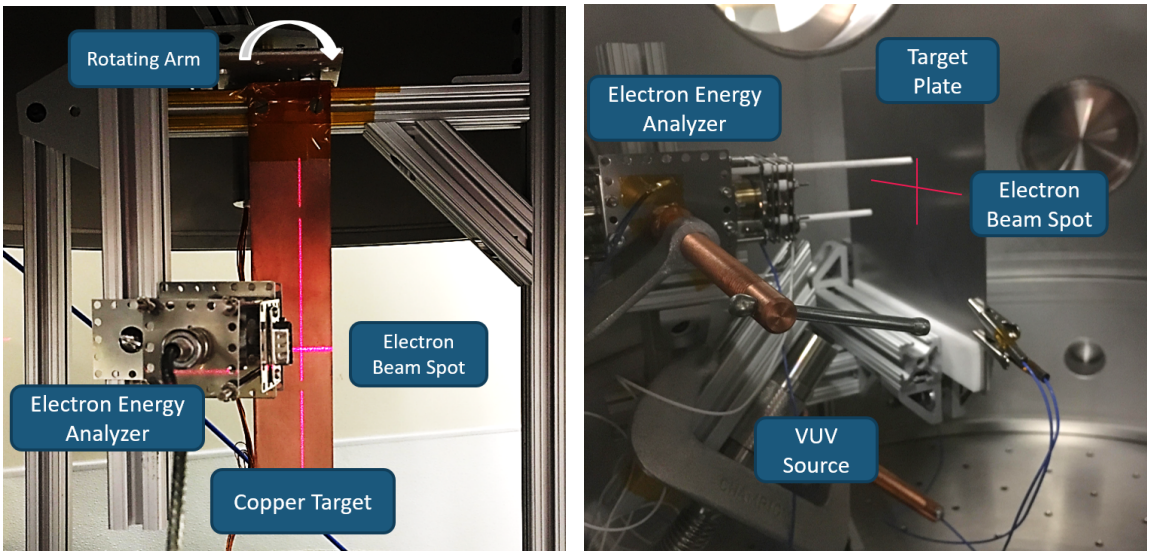

(a) Experiment setup in Minion at AFRL. **(b) Experiment setup in ECLIPS in the AVS Laboratory.**

Fig. 3 Pictures of both setups which were a part of the experimental campaign.

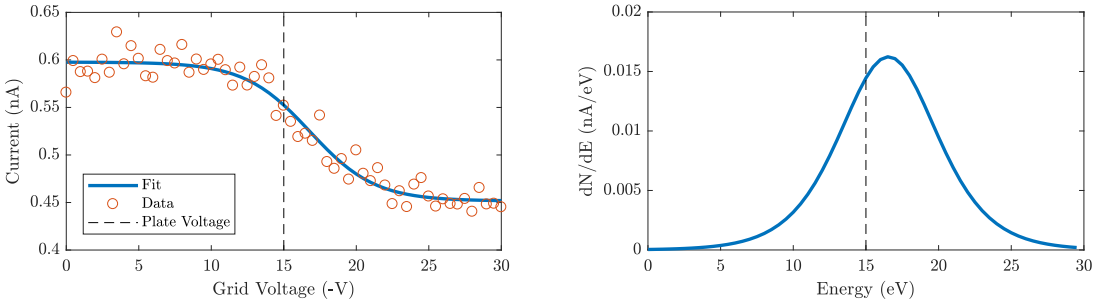

(a) Raw data and model fit of electron current. **(b) Electron energy distribution.**

Fig. 4 Touchless sensing data using secondary electrons with a copper target. The dashed black line is the voltage applied to the target plate.

distribution of the electron population, which has the following form:

$$-\frac{dI}{dV} = bc\left(1 - \tanh^2(cV + d)\right). \tag{2}$$

There is a clear peak in the electron energy distribution near the expected energy (the voltage applied to the plate, designated by the black, dashed line) for all of the materials tested. This provides a proof of concept and demonstrates that touchless potential sensing is feasible for a variety of common spacecraft surface materials. A number of interesting features are present in the data. In each case, the peak of the energy distribution is 2 to 3 volts different from the voltage applied to the plate. With the exception of the secondaries emitted from the copper, the peak is a few volts less than the plate voltage. If an electron were generated on the target surface with exactly zero energy, it would arrive at the detector with an energy exactly equal to the potential of the plate. Any electrons born with energies of a few eVs would arrive with energies slightly higher than the plate potential. Therefore, it is expected that the peak be just above the plate potential. There are several possible mechanisms which could cause the peak to appear at a lower energy. Experiments have shown that localized potential variations on the order of a volt can occur on surfaces because of contaminants or imperfections [21]. Another factor results from the finite spacing between the wires in the discriminator grid. Though each wire is held at the commanded voltage, the area in between wires has a voltage slightly less than the nominal voltage. Additionally, imperfections in the discriminator grid, such as non-uniform flatness and minor kinks or bends

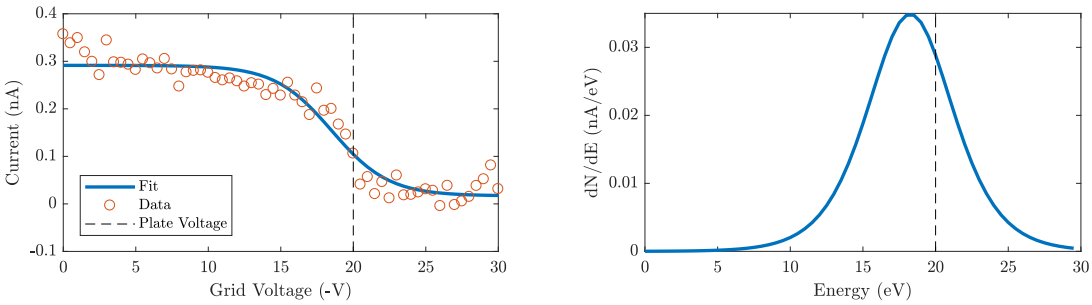

(a) Raw data and model fit of electron current. **(b) Electron energy distribution.**

Fig. 5 Touchless sensing data using photoelectrons with a copper target. The dashed black line is the voltage applied to the target plate.

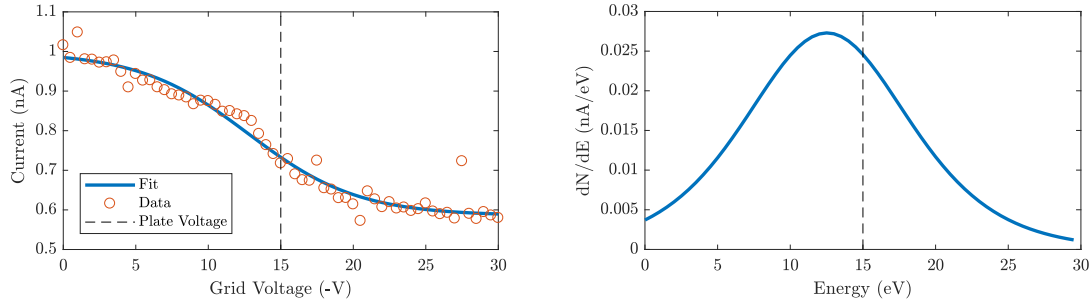

(a) Raw data and model fit of electron current. **(b) Electron energy distribution.**

Fig. 6 Touchless sensing data using secondary electrons with an aluminum target. The dashed black line is the voltage applied to the target plate.

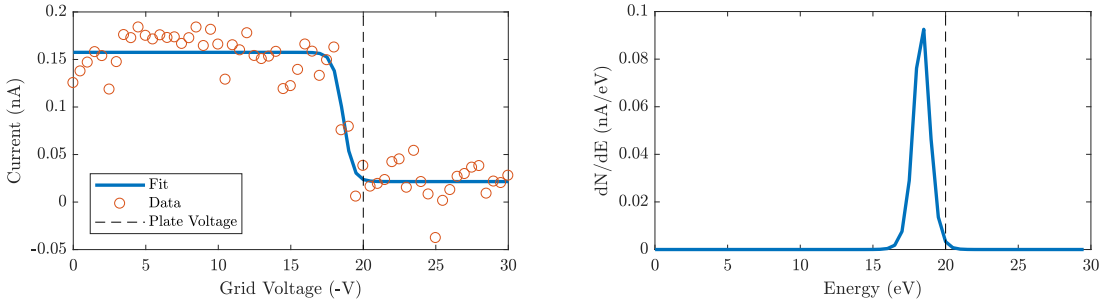

(a) Raw data and model fit of electron current. **(b) Electron energy distribution.**

Fig. 7 Touchless sensing data using photoelectrons with an aluminum target. The dashed black line is the voltage applied to the target plate.

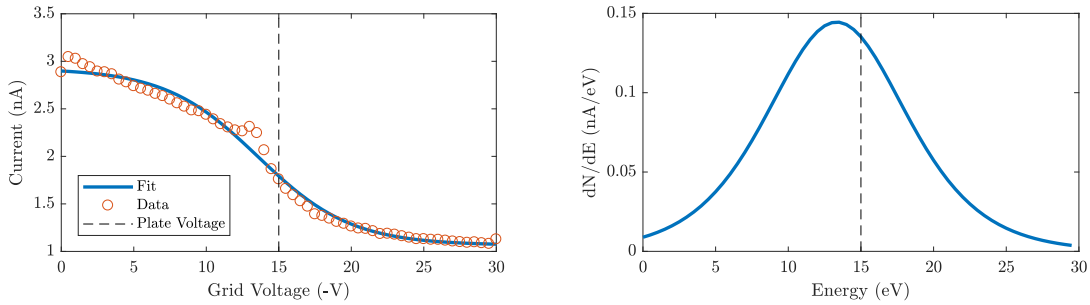

(a) Raw data and model fit of electron current. **(b) Electron energy distribution.**

Fig. 8 Touchless sensing data using secondary electrons with a titanium target. The dashed black line is the voltage applied to the target plate.

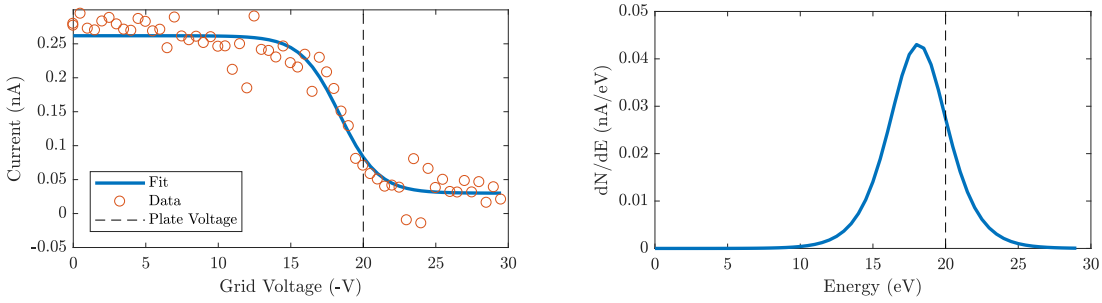

(a) Raw data and model fit of electron current. **(b) Electron energy distribution.**

Fig. 9 Touchless sensing data using photoelectrons with a titanium target. The dashed black line is the voltage applied to the target plate.

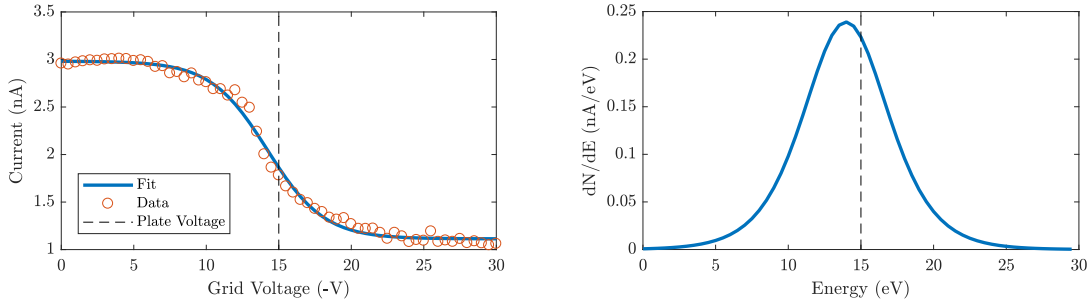

(a) Raw data and model fit of electron current. **(b) Electron energy distribution.**

Fig. 10 Touchless sensing data using secondary electrons with an aluminized Kapton target. The dashed black line is the voltage applied to the target plate.

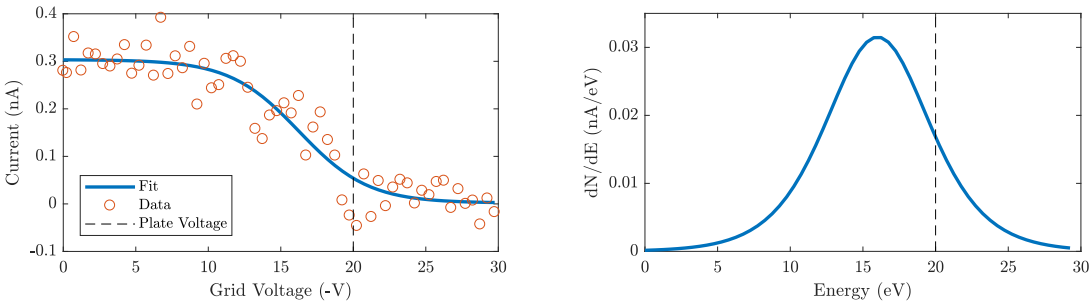

(a) Raw data and model fit of electron current. **(b) Electron energy distribution.**

Fig. 11 Touchless sensing data using photoelectrons with an aluminized Kapton target. The dashed black line is the voltage applied to the target plate.

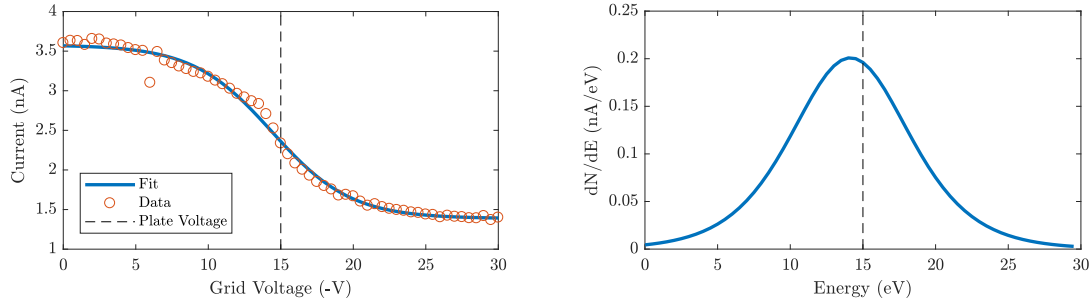

(a) Raw data and model fit of electron current. **(b) Electron energy distribution.**

Fig. 12 Touchless sensing data using secondary electrons with an ITO-coated glass target. The dashed black line is the voltage applied to the target plate.

can allow electrons that have energies less than the nominal grid voltage to pass. The downward shift in energy of the electron population is likely caused by a combination of these factors. The end application of this research is to measure potentials of spacecraft in GEO, which commonly charge to 100s of volts. Spacecraft potentials in the kilovolt range are required for Coulomb actuation missions. Variations on the order of volts are negligible for such applications and may even be smaller than the resolution of the electron energy analyzer. Another interesting feature is that the I-V curve is not flat at low grid voltages, as seen in Figures 6, 8, and 12, but rather has a small negative slope. This indicates that there is a population of electrons with energies between zero volts and the plate voltage. The front grid of the instrument is biased to -10 V, which excludes low energy electrons from entering. These electrons could be secondaries generated in between the first and second grids. Additionally, secondaries generated from elsewhere in the chamber could leak through the side of the detector in between the grids, therefore contributing to this population.

A control test was conducted to measure the noise floor of the system with the electron gun and VUV source turned off. Bias voltages of -15 V and -10 V were applied to the target plate and front grid, respectively, while the discriminator grid voltage was swept from 0 to -30 V. The collected noise has a mean of -0.0083 nA and a standard deviation of 0.045 nA. For the samples tested under electron or ultraviolet irradiation, the collected current is on the order of 0.1 to 1 nA. Therefore, much of the noise observed in the data is a result from operating near the noise floor of the measurement system.

Another factor to consider is how the landing energy of the primary electrons on the target object affects the signal of secondary electrons received by the sensing craft. Whereas the secondary electron yield decreases with increasing primary energy (at incident energies beyond the peak yield), the backscattered electron yield remains relatively constant at increasingly high energies [22]. Further, backscattered electrons have energies up to the incident energy, thus they do not carry information about the surface potential of the target. Therefore, the servicing craft must emit an electron beam at an energy which results in a large number of secondaries. The beam energy selected for the experiment was 1.5 keV. At this incident energy, all of the materials under consideration have secondary electron yields between 1.2 and 1.9 [19, 23],

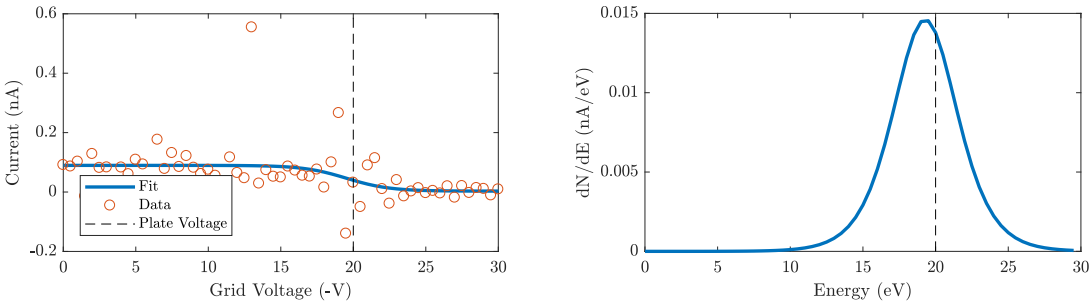

(a) Raw data and model fit of electron current.

(b) Electron energy distribution.

Fig. 13 Touchless sensing data using photoelectrons with an ITO-coated glass target. The dashed black line is the voltage applied to the target plate.

so there are many more secondaries than backscattered electrons. The situation is simpler for photoelectrons; the photon landing energy is determined only by the wavelength of the light and the number of photoelectrons is determined by the intensity of the light. Both photoelectrons and secondary electrons may be observed simultaneously for applications using an electron beam while operating in sunlight.

B. Angle-Energy Resolved Measurements

Measurements were taken to determine the angle relative to the charged, flat plate over which the secondary electron peak can be observed. The electron energy analyzer was mounted to a rotating arm so that it was always facing the plate. The arm was driven by a stepper motor. Note that measurements were taken at discrete steps and only when the system was at rest. The detector front grid was 21 cm away from the copper target, which was maintained at -40 V. The results are shown in Figure 14. Under the given conditions, the secondary electron peak is clearly visible as the sensor moves to approximately 30° off the axis normal to the plate. The signal is too small to be clearly recognized beyond this angle.

The detected signal is a function of the relative distance and potential between the two craft, as discussed in [13]. For target potentials larger in magnitude, the electric field directed away from the surface will dominate the electron trajectory, such that the initial electron velocities parallel to the surface will be negligible. This has the effect of narrowing the angular range in which a sufficiently large signal can be measured. In the current experiment, the maximum magnitude target potential is limited by the available power supplies. Future experiments will utilize high-voltage power supplies to determine how the observable angular range varies with target potential. Similarly, the detected signal also decreases with increasing distance from the target. This occurs because the secondary or photo electron beam expands into a larger volume. Though the physical size of vacuum chambers limits the feasibility of exploring this process further, simulations have been developed to provide insight into the distances over which touchless potential sensing is possible [13].

V. Conclusion

The experimental results presented show that the touchless potential sensing concept is feasible with both secondary and photo electrons for a variety of commonly used materials. Though the surface conditions of materials are known to affect the emission characteristics, the potential is able to sensed accurately for all of the samples under consideration. The peak of the electron energy distribution is within 3 eV of the nominal target potential for all cases. In applications relevant to this topic, spacecraft have surface potentials significantly larger in magnitude than the potentials used in this experiment. Therefore, the technique is capable of providing accurate measurements of surface potential without requiring physical contact. The results of this work have important implications for future missions which seek to employ Coulomb forces and torques between multiple satellites. Future experiments should build upon results with the flat plate target by considering realistic satellite geometries. The electric field around some satellite shapes may only allow for voltage sensing at specific relative attitudes. Therefore, it would be advantageous to implement a surface potential state estimator to optimally fuse periodic measurements with known spacecraft charging physics.

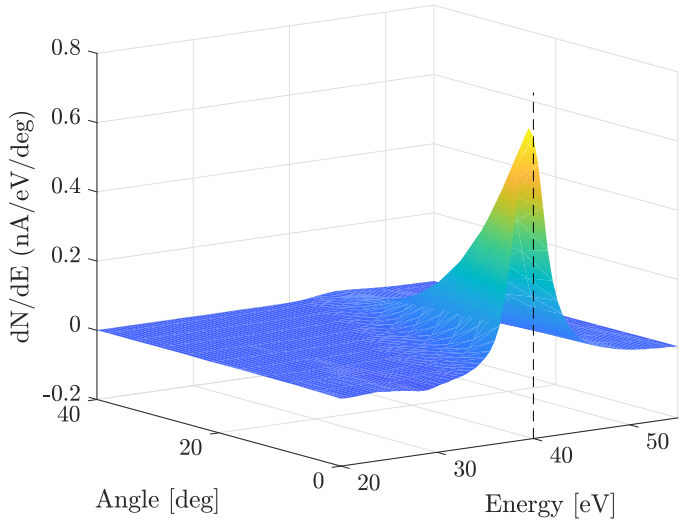

Fig. 14 Angle-resolved touchless sensing experiment results for a copper target. The dashed black line indicates the potential difference between the target and the sensor of -40 V.

Acknowledgments

The authors would like to thank Jordan Maxwell, Kieran Wilson, Joseph Hughes, Zoltan Sternovsky, Ryan Hoffman, and Dan Engelhart for fruitful discussions on the topic of touchless sensing. Additionally, we would like to thank Luis Hernandez, Dalton Turpen, and Adrian Stang for assistance with machining, assembling, and troubleshooting various components of the experiments.

References

[1] Ferguson, D. C., Denig, W. F., and Rodriguez, J. V., "Plasma Conditions During the Galaxy 15 Anomaly and the Possibility of ESD from Subsurface Charging," *AIAA Aerospace Sciences Meeting including the New Horizons Forum and Aerospace Exposition*, Orlando, FL, 2011. Paper AIAA 2011-1061.

[2] O'Brien, T., "SEAES-GEO: A spacecraft environmental anomalies expert system for geosynchronous orbit," *Space Weather*, Vol. 7, No. 9, 2009, pp. 1–14.

[3] Ferguson, D. C., "Charging of the International Space Station due to its High Voltage Solar Arrays," *NASA Technical Report*, 2002.

[4] Anderson, P. C., "Characteristics of spacecraft charging in low Earth orbit," *J. Geophys. Res.*, Vol. 117, No. A7, 2012, p. A07308. doi:10.1029/2011JA016875, URL `http://dx.doi.org/10.1029/2011JA016875`.

[5] Ogilvie, A., Allport, J., Hannah, M., and Lymer, J., "Autonomous satellite servicing using the orbital express demonstration manipulator system," *Proc. of the 9th International Symposium on Artificial Intelligence, Robotics and Automation in Space (i-SAIRAS'08)*, 2008, pp. 25–29.

[6] Xu, W., Liang, B., Li, B., and Xu, Y., "A universal on-orbit servicing system used in the geostationary orbit," *Advances in Space Research*, Vol. 48, No. 1, 2011, pp. 95–119. doi:10.1016/j.asr.2011.02.012, URL `http://www.sciencedirect.com/science/article/pii/S0273117711001402`.

[7] Ellery, A., Kreisel, J., and Sommer, B., "The case for robotic on-orbit servicing of spacecraft: Spacecraft reliability is a myth," *Acta Astronautica*, Vol. 63, No. 5-6, 2008, pp. 632–648.

[8] Bengtson, M., Wilson, K., Hughes, J., and H, S., "Survey of the Electrostatic Tractor Research for Reorbiting Passive GEO Space Objects," *Astrodynamics*, 2018.

[9] Bennett, T., and Schaub, H., "Touchless Electrostatic Three-Dimensional Detumbling of Large Axi-Symmetric Debris," *Journal of Astronautical Sciences*, Vol. 62, No. 3, 2015, pp. 233–253.

[10] Schaub, H., and Parker, G. G., "Constraints of Coulomb Satellite Formation Dynamics: Part I – Cartesian Coordinates," *Proceedings of the Institution of Mechanical Engineers, Part G, Journal of Aerospace Engineering*, 2006. Accepted for publication.

[11] Ferguson, D. C., Murray-Krezan, J., Barton, D. A., Dennison, J., and Gregory, S. A., "Feasibility of detecting spacecraft charging and arcing by remote sensing," *Journal of Spacecraft and Rockets*, Vol. 51, No. 6, 2014, pp. 1907–1913.

[12] Wilson, K., and Schaub, H., "Remote Sensing of Spacecraft Electrostatic Potential Using Bremmstrahlung," *The 15th Spacecraft Charging and Technology Conference*, 2018.

[13] Bengtson, M., Hughes, J., and Schaub, H., "Remote Sensing of Spacecraft Electrostatic Potential Using Secondary Electrons," *The 15th Spacecraft Charging and Technology Conference*, 2018.

[14] Mullen, E. G., Gussenhoven, M. S., Hardy, D. A., Aggson, T. A., and Ledley, B. G., "SCATHA Survey of High-Voltage Spacecraft Charging in Sunlight," *Journal of Geophysical Research*, Vol. 91, No. A2, 1986, pp. 1474–1490. doi:10.1029/JA091iA02p01474.

[15] Halekas, J., Mitchell, D., Lin, R., Hood, L., Acuña, M., and Binder, A., "Evidence for negative charging of the lunar surface in shadow," *Geophysical research letters*, Vol. 29, No. 10, 2002.

[16] Halekas, J., Delory, G., Lin, R., Stubbs, T., and Farrell, W., "Lunar Prospector observations of the electrostatic potential of the lunar surface and its response to incident currents," *Journal of Geophysical Research: Space Physics*, Vol. 113, No. A9, 2008.

[17] Halekas, J., Delory, G., Lin, R., Stubbs, T., and Farrell, W., "Lunar Prospector measurements of secondary electron emission from lunar regolith," *Planetary and Space Science*, Vol. 57, No. 1, 2009, pp. 78–82.

[18] Chung, M., and Everhart, T., "Simple calculation of energy distribution of low-energy secondary electrons emitted from metals under electron bombardment," *Journal of Applied Physics*, Vol. 45, No. 2, 1974, pp. 707–709.

[19] Baglin, V., Bojko, J., Scheuerlein, C., Gröbner, O., Taborelli, M., Henrist, B., and Hilleret, N., "The secondary electron yield of technical materials and its variation with surface treatments," Tech. rep., 2000.

[20] Bruining, H., *Physics and Applications of Secondary Electron Emission: Pergamon Science Series: Electronics and Waves—a Series of Monographs*, Elsevier, 1954.

[21] Robertson, S., Sternovsky, Z., and Walch, B., "Reduction of asymmetry transport in the annular penning trap," *Physics of Plasmas*, Vol. 11, No. 5, 2004, pp. 1753–1756.

[22] Lai, S. T., *Fundamentals of Spacecraft Charging: Spacecraft Interactions with Space Plasmas*, Princeton University Press, 2011.

[23] Krainsky, I., Lundin, W., Gordon, W., and Hoffman, R., "Secondary electron emission yields," 1981.